



In-Vitro Anticancer Activity of Chemical Constituents from *Etlingera alba* Poulsen against Triple Negative Breast Cancer and in silico Approaches towards Matrix metalloproteinase-1 Inhibition

W. Wahyuni^{1,2}, Ajeng Diantini^{1,*}, Mohammad Ghozali¹, Anas Subarnas¹, Euis Julaeha¹, Riezki Amalia¹, Adryan Fristiohady^{2,3}, Andini Sundowo⁴, Sofa Fajriah⁴, Yuni Elsa Hadisaputri¹, Raden Maya Febrianti¹, Fauzia Azzahra¹, Agung W.M. Yodha⁵, I. Sahidin²

¹Universitas Padjadjaran, Jatinangor, Indonesia

²Universitas Halu Oleo, Kendari, Indonesia

³Thammasat University, Pathum Thani, Thailand

⁴National Research and Innovation Agency (BRIN), Kawasan Puspitek, Tangerang Selatan 15314, Indonesia

⁵Politeknik Bina Husada, Kendari, Indonesia

Correspondence: E-mail: ajeng.diantini@unpad.ac.id

ABSTRACT

Etlingera alba (EA) is one of the endemic plants grown in Sulawesi. We determined the cytotoxic and anti-metastatic activity of isolates obtained from EA rhizome extract. IC₅₀ value for 1,7-diphenyl-6-heptene-3-one, sitostenone, sinapyl alcohol diacetate, and sinapyl alcohol acetate were 134.59; 170 ; 128.11; and 161.96 $\mu\text{g}/\text{mL}$, respectively. The compounds also had anti-migration activity. 200- $\mu\text{g}/\text{mL}$ Sitostenon exhibited the lowest migration rate (3.32%). The free bond energies of sitostenon, 1,7-diphenyl-6-heptene-3-one, sinapyl alcohol acetate, and sinapyl alcohol diacetate were -11.81; -8.25; -6.64; and -6.28 kcal/mol, respectively. All compounds were more effective in stabilizing the Matrix metalloproteinase 1 complex. Isolation from EA rhizomes have the potential to be developed as anti-metastatic for Triple-Negative Breast Cancer.

© 2022 Tim Pengembang Jurnal UPI

ARTICLE INFO

Article History:

Submitted/Received 02 May 2022

First revised 05 Jun 2022

Accepted 08 Aug 2022

First available online 12 Aug 2022

Publication date 01 Sep 2022

Keyword:

Anti-metastatic,
Cytotoxic activity,
Docking,
Etlingera alba,
MDA-MB-231 cell lines,
MMP-1,
Molecular dynamic.

1. INTRODUCTION

Breast cancer is a type of cancer that common among women, with ranks first in new cases and sixth in death in 2020 (Sung et al., 2021). Breast cancer is cancer that occurs in breast tissue. According to data from GLOBOCAN, International Agency for Research on Cancer (IARC) in 2020, breast cancer is one type of cancer that has a fairly high prevalence and is the main cause of morbidity worldwide, which is 11.7% or 2.261 million people and mortality ranks at number one. five, namely 6.9% or 684,996 million people. In Indonesia, the breast cancer morbidity rate ranks first at 16.6%, or 65,858 million people and the mortality rate is 9.6%, or 22,430 million people (Sung et al., 2021).

Cancer is an uncontrolled growth cell with the oncogenes activation and tumor suppression gene deactivation (Sarkar et al., 2013). Triple-Negative Breast Cancer (TNBC) is a type of breast cancer that lacks express estrogen receptor (ER), progesterone receptor (PR), and Human Epidermal Growth Factor Receptor 2 (HER2). It is more aggressive to spread or metastasis and has a poor prognosis than other types of breast cancer (da Silva et al., 2020; Chmielewska-Kassassir et al., 2020).

Tumor invasion as the first step of metastasis generally requires the breakdown of the extracellular matrix by proteolytic enzymes. Cancer cells form protruding invadopodia that generate and relieve matrix metalloproteinases (MMPs), which degrade the basement membrane and allow metastasis. Matrix metalloproteinase 1 (MMP-1) is a member of the zinc-dependent endopeptidase family which overexpressed in TNBC. It has a vital role in the metastasis process of breast cancer. It is proposed for TNBC treatment due to its association with breast cancer lymph node metastasis and TNBC. By knocking-down MMP-1, it suppresses the protein expression of c-

Myc, p-AKT, AKT, and Bcl-2 through the P13K/Akt pathway (Wang et al., 2019; Argote Camacho et al., 2021; Liu et al., 2021).

Currently, there is no specific agent for treating TNBC. Therefore, finding anticancer activity, specifically for TNBC agents, is intensively developed with low toxicity and high efficacy. Phytochemical from plants is promising to be developed due to many studies that identify plants' wide range of biological properties, including anti-inflammatory, antioxidant, neuroprotection, and anti-cancer.

Etingera alba is one of the plants belonging to the genus *Etingera* belonging to the Zingiberaceae family. Many species from *Etingera*, including *E. elatior* (Chan et al., 2011; Wahyuni et al., 2019; Fristiody et al., 2020), *E. brevilabrum* (Mahdavi et al., 2014), *E. fulgens* (Nagappan et al., 2019), *E. calophrys* (Sahidin et al., 2018; Sahidin et al., 2022), *E. paviena* (Tachai & Nuntawong 2016), and *E. punicea* (Nagappan et al., 2019) provide pharmacological activity. *E. alba* has pharmacological activity, including anti-inflammatory by reducing rat palm edema and tumor necrosis factor-alpha (TNF- α), Interleukin-6 (IL-6), and Interleukin-12 (IL-12) levels. It also has antibacterial activity against *Escherichia coli* and *Salmonella enterica* (Hamsidi et al., 2021). It is an endemic plant that is mainly found in Sulawesi, thereby potentially exploring its pharmacological activity. *E. alba* rhizome extract has antioxidant activity (Wahyuni et al., 2021a). A fraction from ethanolic extract of *E. alba* rhizome exhibited anticancer and anti-metastatic properties against triple-negative MDA-MB-231 breast cancer cell lines (Wahyuni et al., 2021b). However, a study that discusses the compounds of *E. alba* and its pharmacological activities is still limited in

particular the anticancer activity against specific cancer target MMP-1.

Thus, this study aims to determine the anticancer and anti-metastatic activity of compounds obtained from *Etlingera alba* rhizome in TNBC. The molecular docking and molecular dynamic approach were conducted to confirm and verify the binding efficiency of compounds towards target proteins *in silico*.

2. METHODS

2.1. Plant Material

The rhizome of *Etlingera alba* was obtained from Punggaluku of South Konawe Regency in Southeast Sulawesi. Samples were dried at 40 °C and avoid direct sunlight. The samples were ground and placed in a sealed container for further analysis.

2.2. Cell Lines Preparation and Culture

The MDA-MB-231 cell line collected from the Laboratory of Cell Biology and Molecular, Faculty of Pharmacy Universitas Padjajaran was cultured in a 100 mm plate in a CO₂ incubator and observed under an inverted microscope after 24 h. After that, the cells were seeded in 6 well plates containing fresh media (2 mL) per well. 2x10⁴ cells/well was required for cytotoxicity assay and migration assay, thereby the cells were incubated for 24 h in a CO₂ incubator. After 24 h, the cell distribution was observed whether the cells attained ~70-80% of confluence.

2.3. Material

Silica gel 60 (0.063-0.200 mm) F₂₅₄ Merck, Dulbecco's modified eagle medium (DMEM)-high glucose (Sigma, St. Louis, MO), fetal bovine serum (Sigma), trypsin TrypLE (Gibco, Thermofisher, New York), penicillin-streptomycin (Sigma), phosphate buffer saline 10X (Lonza, Swiss), Cisplatin, and cell counting kit-8 (CCK) reagent (Dojindo, Rockville, MD). 96% ethanol, n-hexane, ethyl acetate (EtOAc), and

methanol (MeOH) used were technical grade.

2.4. Extraction and Fractionation

E. alba rhizome powder (5.5 kg) was extracted with 96% ethanol 3 x @ 20 L, each extraction was conducted for 24 h. The ethanol extract was then concentrated using a vacuum rotary evaporator (Rotavapor R-210 Buchi Germany) at low pressure to form a dark brown gum (150 g). The 96% ethanol extract was then fractionated with VLC (vacuum liquid chromatography) using a column 10 cm, silica gel stationary phase (250 g) and a mixed mobile phase n-hexane:EtOAc (9:1, 8:2, 5:5, 2:8), 100% EtOAc, and 100% MeOH. Fractionation was performed out 6 x @ 25 g, resulting in 6 A-F fractions, respectively 3.24, 4.35, 5.36, 1.56, 4.43 and 74.22 g.

Fraction B in VLC used 5 cm column, silica gel stationary phase (100 g) and a mixed mobile phase of n-hexane:EtOAc (9:1 and 8:2), 100% EtOAc and 100% MeOH, resulting in 4 subfractions B1- B4, 0.85, 1.12, 0.99 and 0.90 g, respectively. Subfraction B1 was further purified using RC/ Radial chromatography (silica gel stationary phase, mobile phase n-hexane:EtOAc (9.5:0.5) and 100% EtOAc), in order to obtain compound 1 (1,7-diphenyl-6-heptene-3-one, 668.6 mg). Purification of subfraction B2 using RC (stationary phase silica gel, mobile phase n-hexane:EtOAc (9:1) and 100% EtOAc) yielded compound 2 (sitostenone, 63.1 mg). Further purification was carried out on the B3 subfraction using RC (silica gel stationary phase, mobile phase n-hexane:EtOAc (8:2) and 100% EtOAc) to produce compound 3 (Sinapyl Alcohol Diacetate, 81 mg). Further purification of fraction B4 using RC (stationary phase silica gel, mobile phase n-hexane:chloroform:MeOH (7:2:1) and 100% EtOAc) yielded compound 4 (Sinapyl Alcohol Acetate, 63.6 mg).

2.5. Structure Identification

In determining the structure of isolated compounds, spectroscopic techniques were used. Spectrums were measured using an FTIR Alpha II-Bruker (Billerica, MA, USA) spectrometer, ^1H NMR and ^{13}C NMR spectra were determined using a JEOL JNM-ECZ500R/S1 (Japan) FT NMR spectrometer, operating at 500.159 MHz (1H) and 125,765 MHz (13C). LC-MS/MS analysis used Xevo G2-XS QTOF (Waters Corporation, Milford, USA) to determine the mass.

2.6. Cytotoxic Activity Assay

The MDA-MB-231 cell lines were seeded in 96 well microplates and incubated for 24 h in a CO_2 incubator. From that point forward, the media were supplanted and added with 10 μl of fresh media containing various concentrations of sample, and Cisplatin as the control followed by incubating in various periods (6, 12, 24, and 48 h) in a CO_2 incubator. After incubation, the Cell Counting Kit-8 (CCK-8) reagent (Dojindo, Rockville, MD, USA) was added to each well of 96 well microplates and continued to be placed in a CO_2 incubator for 4 h to react. Then, the absorbances were measured with a microplate reader (Tecan Infinite spectrophotometer) at a wavelength of 450 nm. The survival rate (%) of cells was calculated using Eq. (1).

$$\text{Survival rate} = \left(\frac{A_{\text{sample}} - A_{\text{blank}}}{A_{\text{control}} - A_{\text{blank}}} \right) \times 100\% \quad (1)$$

where A_{sample} is the sample's absorbance, A_{blank} is the blank's absorbance, and A_{control} is the control's absorbance.

2.7. Migration Cell Assay

After confluences, the culture was washed using PBS, replaced the medium with a fresh medium, added 2 mL of 0.5% FBS, and incubated in a CO_2 incubator at 37°C for 24 h. After incubation, the scratch

was conducted using a sterile yellow tip in an upright position, and then the all-growth media were discarded and washed with PBS on the plate. The step was continued by adding the sample with various concentrations and immediately photographed as the 0 h. The cultures were treated and put in in CO_2 incubator (37°C) for 24 h and photographed for 24 h with the same magnification. Cell count performed with hemocytometer according to cell calculation protocol.

The migration percentage (%) was calculated using Eq. (2).

$$\text{Migration percentage} = \left(\frac{\text{diameter at 0 h} - \text{diameter at 24 h}}{\text{diameter at 0 h}} \right) \times 100\% \quad (2)$$

where *diameter at 0 h* means the gaps of the cell after being treated at 0 h. *Diameter at 24 h* means the gaps of cells after being treated at 24 h.

2.8. Protein and Ligand Preparation

We selected the three-dimensional structure of matrix metalloprotease-1 (MMP-1) from Protein Data Bank (PDB ID: 966C) (<https://www.rcsb.org/>). The compounds and cisplatin data were collected from the PubChem database (<https://pubchem.ncbi.nlm.nih.gov/>). The protein and ligands were prepared in AutoDockTool 1.5. (Morris et al., 2009). The protein was treated by removing water molecules and adding protonations and the Kollman charge. Meanwhile, the ligand was designed to rotate freely and add the Gasteiger charge

2.9. Molecular Docking Simulation

The docking process was run with the assistance of AutoDock software (Morris et al., 2008). The binding site is set following the RS2 position as a native ligand on the x, y, and z-axis with a grid area of 40 x 40 x 40 Å and 0,375 Å point spacing. The docking parameter applies the Genetic Algorithm run as 100, population size as 150, and the maximum number of evaluations was set

to 2,500,000. Then, the platinum metal (Pt) parameter was added for cisplatin, and the other parameters were set to default. The interactions of each molecule were then visualized with Discovery Studio Visualizer software.

2.10. Molecular Dynamics Simulation

Molecular dynamics simulations were performed with the help of GROMACS 2016 (Abraham *et al.*, 2015). The AMBER99SB-ILDN force field was applied to parameterize the MMP-1 (Petrov & Zagrovic, 2014). Parametric files of molecules were constructed using ACPYPE (Sousa da Silva *et al.*, 2012). The system was neutralized by adding Na and Cl ions, and the TIP3P water model was applied for the solvation process. The pressure and temperature are set to 1 atm and 310 K. The long-range electrostatic force mimics

the Particle Mesh Ewald method (Wang *et al.*, 2016). The stability of the systems was verified by analyzing the root-mean-square deviation and fluctuations (RMSD and RMSF), H-bonds Occupancy, principal component analysis (PCA), solvent accessible surface area (SASA), and radius of gyration (*Rg*). The binding energies were also determined using the MM/PBSA method with the help of the *g_mmpbsa* package (Kumari & Kumar, 2014).

3. RESULTS

3.1. Structure Identification

The structure of the compound was determined by identifying the MS spectrum, IR spectrum, and NMR spectroscopy. The spectrums were compared with the reference (see Figure 1).

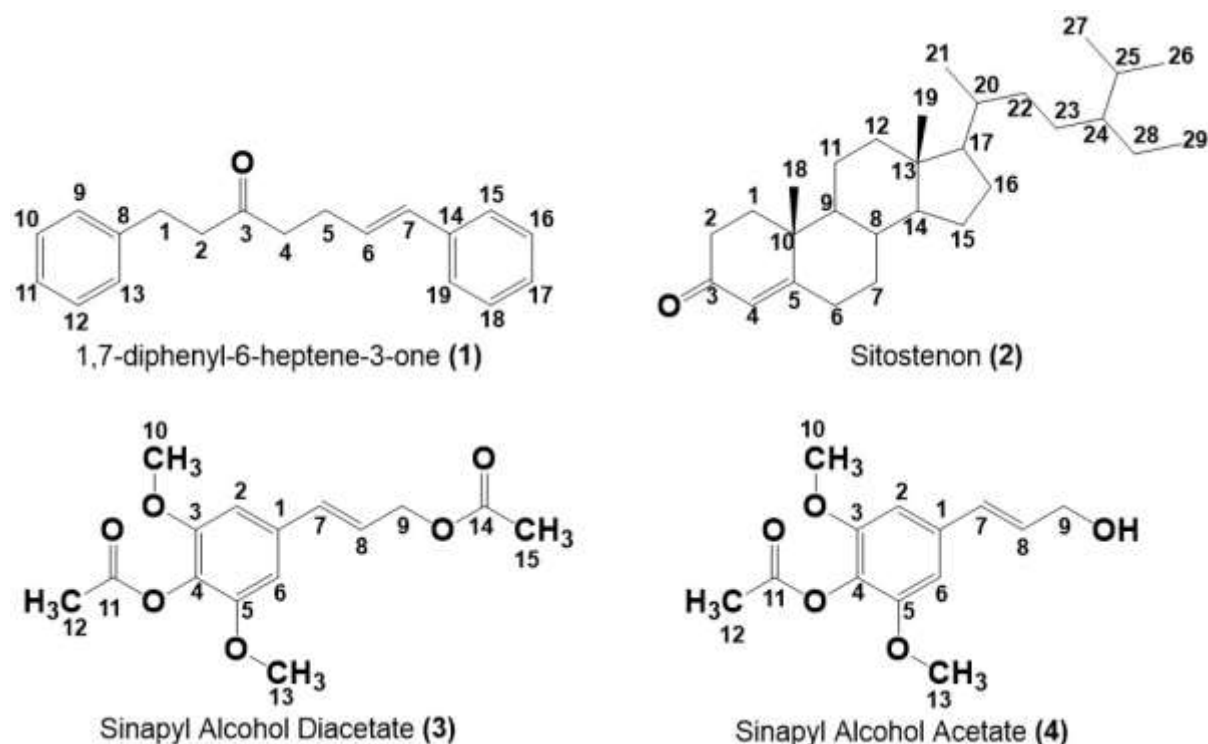


Figure 1. The metabolites isolated from etlingera alba rhizome : (1) 1,7-diphenyl-6-heptene-3-one; (2) Sitostenon; (3) Sinapyl alcohol diacetate; (4) Sinapyl alcohol acetate.

The structure interpretation of 4 compounds was conducted by identifying the functional groups through the information indicated by the IR band in **Figure 2**. The FTIR bands of compounds 1-4 in the KBr pellet exhibited the maximum wave number (see **Table 1**). According to [Nandiyanto et al. \(2019\)](#), [Obinna \(2022\)](#), and [Sukamto & Rahmat \(2023\)](#), the peaks might be corresponded to:

- (i) The sharp absorption intensity in the area of 3552 cm^{-1} in compound 4 indicated the presence of a group associated with oxygen (OH), namely alcohol.
- (ii) Bands at areas 3026 cm^{-1} (compound 1), 3027 cm^{-1} (compound 3), and 3022 cm^{-1} (compound 4) confirmed the presence of unsaturated olefinic C-H groups.
- (iii) The band shown at $2970\text{--}2815\text{ cm}^{-1}$ indicated the identification of the aliphatic C-H group. Long-chain linear aliphatic C-H groups were followed by

peaks at 1446 cm^{-1} (compound 1) and 1441 cm^{-1} (compound 2).

- (iv) The range between $1750\text{--}1700\text{ cm}^{-1}$ describes simple carbonyl groups such as ketones, aldehydes, esters, or carboxylates. The ketone group was identified at 1714 cm^{-1} (compound 1) and 1706 cm^{-1} (compound 2), while the ester group was identified at 1731 cm^{-1} (compound 3) and 1730 cm^{-1} (compound 4).
- (v) The band between 1615 and 1495 cm^{-1} in compounds 1, 2, and 3 was the response of the C=C bond in the aromatic ring. A band follows this band in the area between 3150 and 3000 cm^{-1} .
- (vi) The absorption band of the aromatic ring is also supported by the emergence of moderate to solid absorption intensity in the area between $850\text{--}670\text{ cm}^{-1}$, namely the identification of aromatic C-H buckling vibrations.

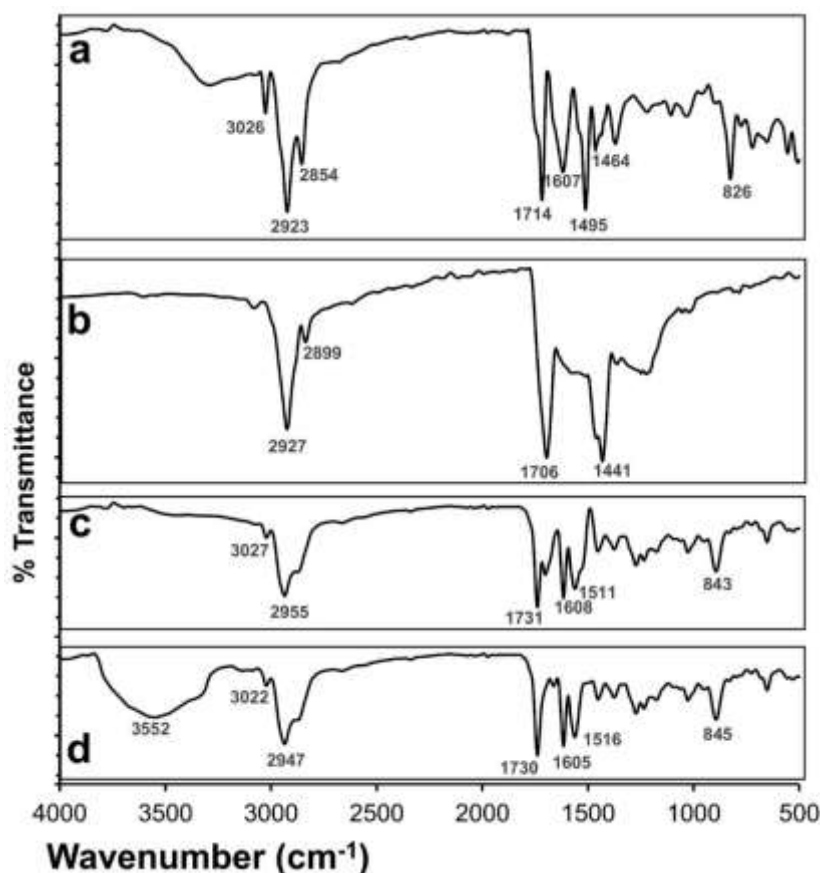


Figure 2. The FTIR spectra of compounds 1 (A); 2 (B), 3 (C), and 4 (D).

Table 1. The FTIR spectra of compounds 1-4.

No	Wavenumber (cm ⁻¹)				Functional Group
	Compound 1	Compound 2	Compound 3	Compound 4	
1	-	-	-	3552	O-H alcohol
2	3026	-	3027	3022	C-H olefinic
3	2923	2928	2955	2947	C-H aliphatic
4	2854	2899	-	-	C-H aliphatic
5	1714	1706	-	-	C=O ketone
6	-	-	1731	1730	C=O ester
7	1605	-	1608	1605	C=C aromatic ring
8	1495	-	1511	1516	C=C aromatic ring
9	1464	1441	-	-	C-H aliphatic
10	826	-	843	845	C-H aromatic

The structure of the isolated compound was further confirmed by interpreting proton and carbon NMR data (**Figures 3 - 5**). Proton NMR provides information about signal count, multiplicity, signal integration, chemical shift (δ), and coupling constant (J). The interpretation of the structure of proton NMR compounds was as follows:

- (i) Identified the number of signals that appeared by observing the chemical environment of the structure of the compounds analyzed. The signal represents the difference in the chemical environment of the hydrogen atoms in a molecule.
- (ii) Identified the multiplicity that arose due to neighboring protons. Multiplicity describes a proton's environment with other adjacent protons.
- (iii) Identified the signal integration value indicating the relative amount of H obtained from measuring the length of each peak.
- (iv) Peak identification based on the value of chemical shift (δ) appears as a result of the presence of electrons in a molecule that forms a shielding effect on the spin of the nucleus
- (v) Identified the coupling constant (J) that reflects the presence of the nuclear bonding environment
- (vi) From steps 1-5, it was concluded that the structural data of the compounds

were then compared with the literature.

In contrast to proton NMR, the absorption peaks shown at carbon NMR (**Figure 4**) provide structural information based on the chemical shifts of different types of carbon in chemical compounds. The steps in determining the structure of a compound are as follows:

- (i) The number of carbon atoms (C) can be determined by looking at the number of peaks that appear and the chemical environment of the carbon
- (ii) Identify the chemical shift value (δ) that appears to predict the type of carbon
- (iii) Determine the molecular formula, which was then compared with the literature.

The results of the proton NMR analysis get the number and types of protons present in the compound structure. Then, carbon NMR analysis obtains information about the number and type of bonding of carbon atoms. Thus, the structure of a compound was determined by combining the proton NMR and carbon NMR results (**Table 2**) which are compared with the literature. Based on spectra data, compound 1 is identical to 1,7-diphenyl-6-heptene-3-one, compound 2 is sitostenone ([Sahidin et al., 2022](#)), compound 3 is Sinapyl Alcohol Diacetate, and compound 4 is Sinapyl Alcohol Acetate ([Jabbar et al., 2021](#)).

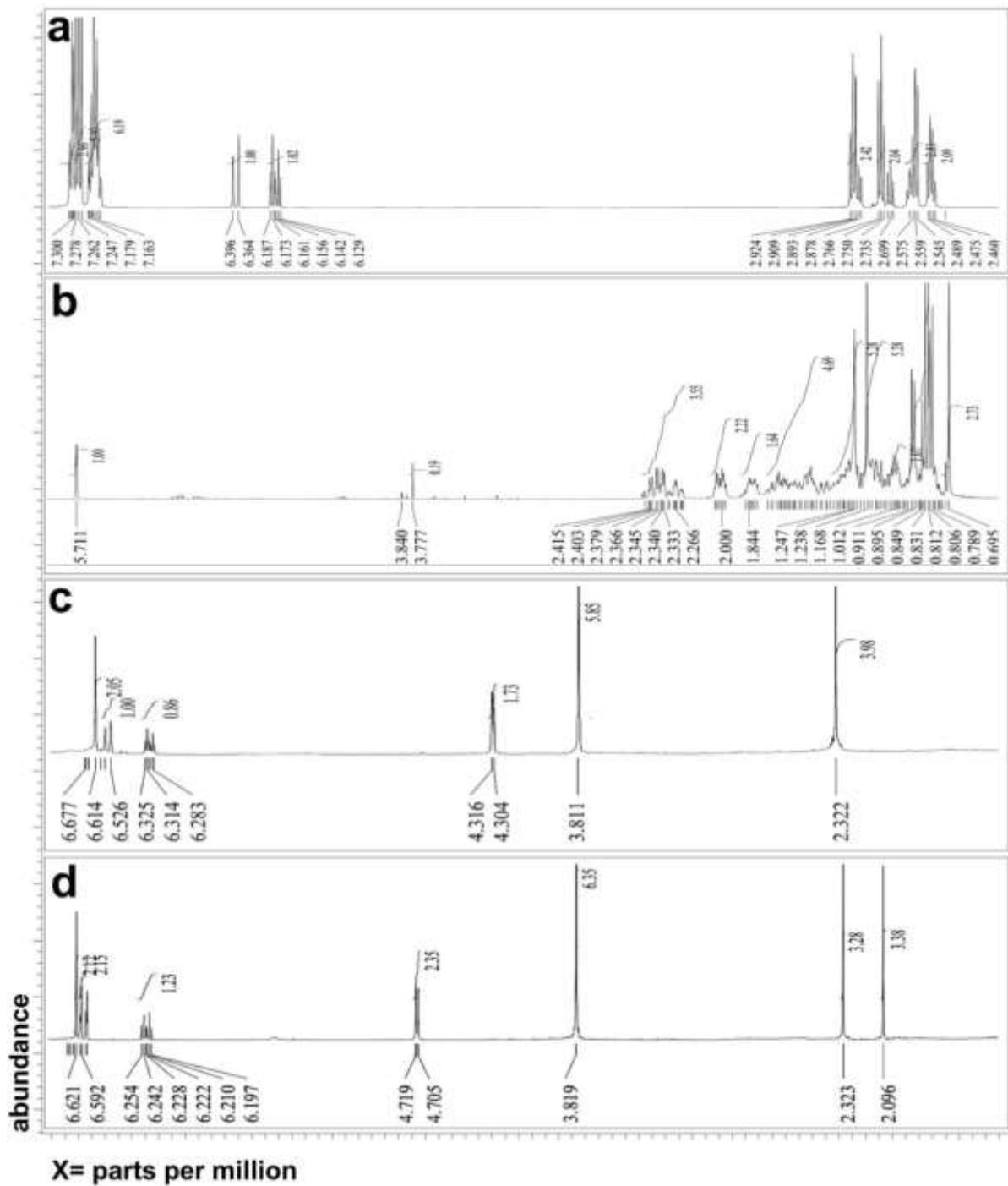


Figure 3. The ^1H NMR Spectra of Compounds 1 (a); 2 (b), 3 (c), and 4 (d).

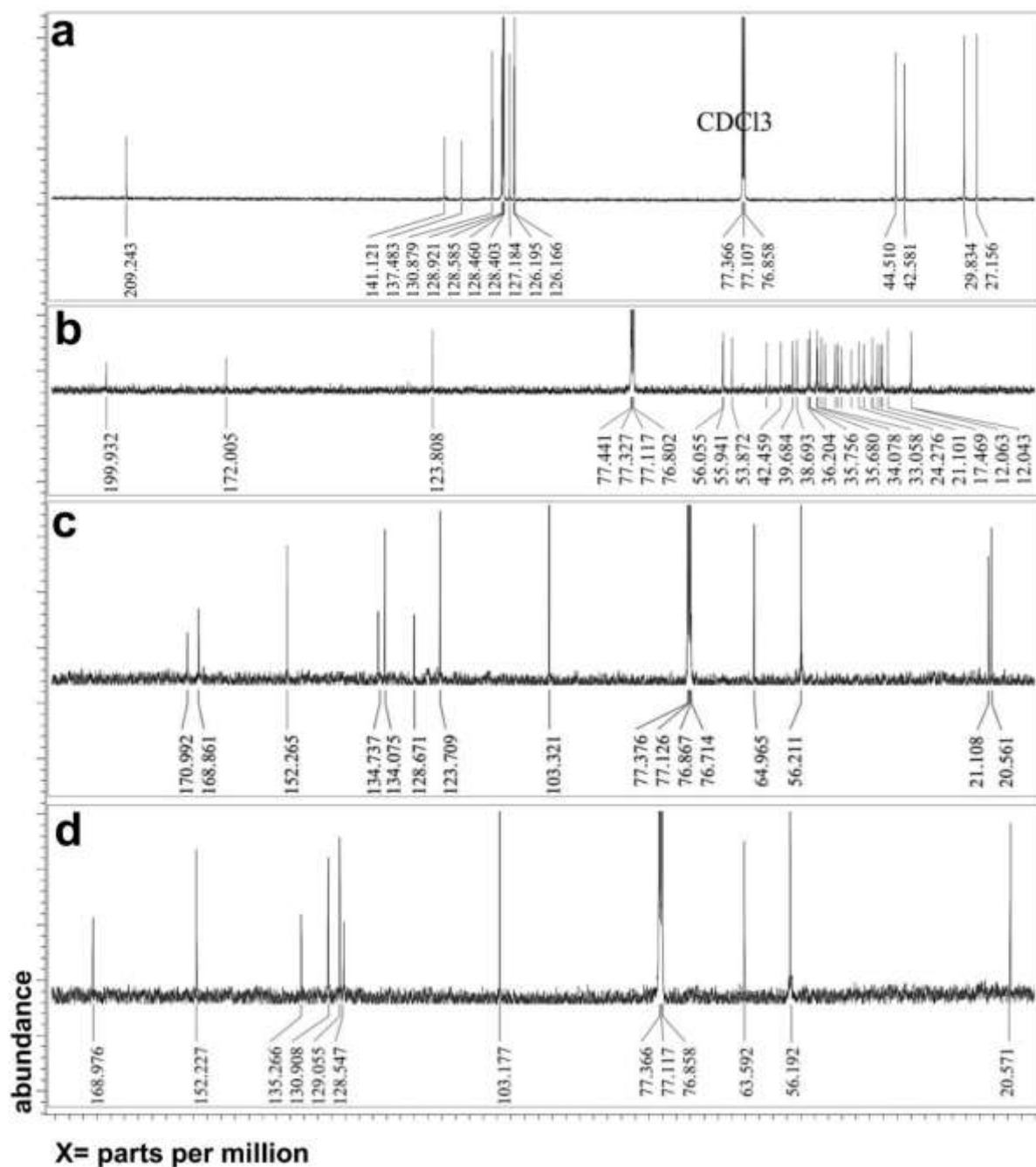


Figure 4. The ¹³C NMR Spectra of Compounds 1 (a); 2 (b), 3 (c), and 4 (d).

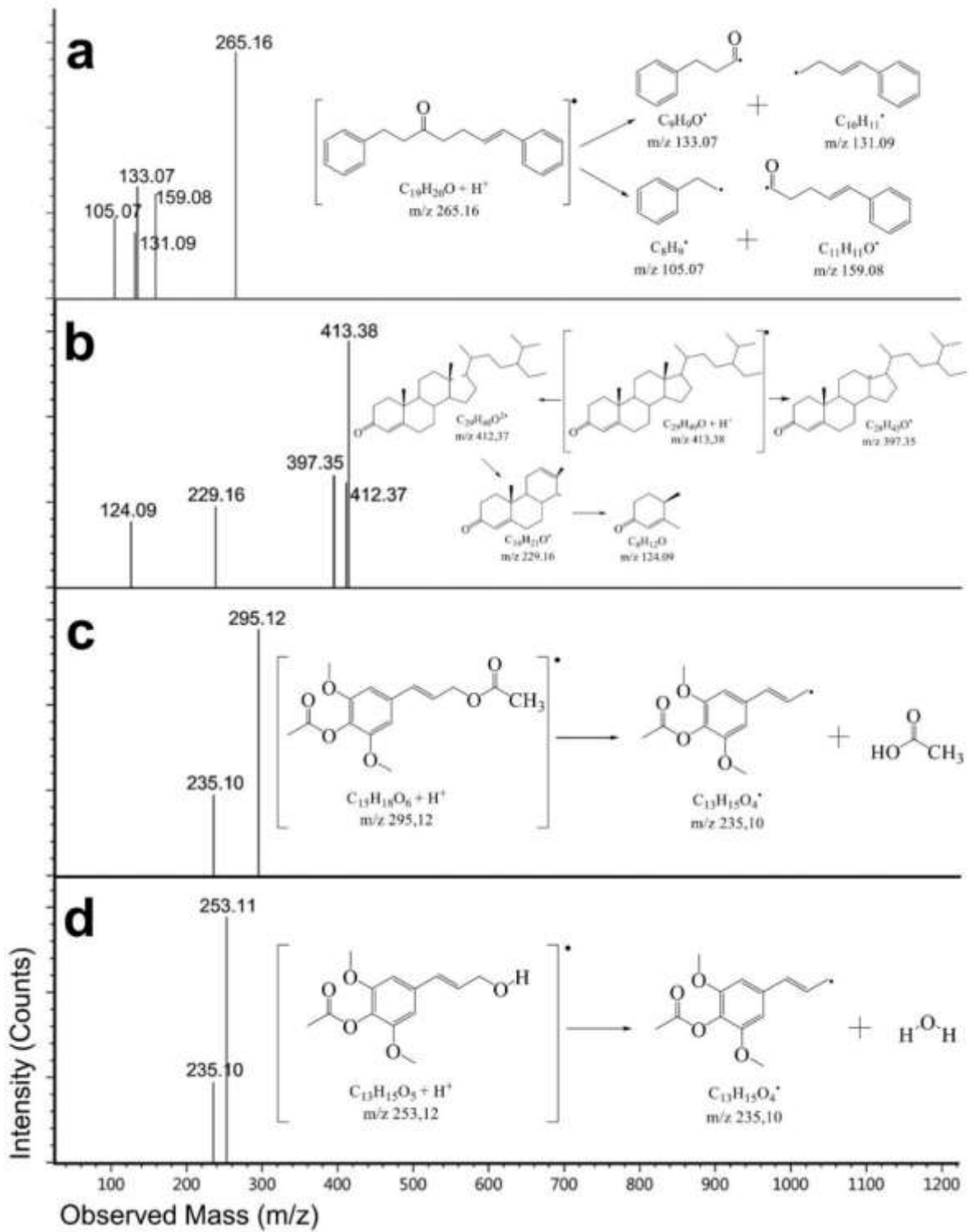


Figure 5. The mass spectra of compounds 1 (a); 2 (b), 3 (c), and 4 (d).

Table 2. The ^1H and ^{13}C NMR spectra of compounds 1-4.

C	Compound 1			Compound 2			Compound 3			Compound 4		
	δ_c	δ_H	(ΣH , m, J (Hz))	δ_c	δ_H	(ΣH , m, J (Hz))	δ_c	δ_H	(ΣH , m, J (Hz))	δ_c	δ_H	(ΣH , m, J (Hz))
1	29.8	2.91	(2H, t, 7.5)	35.7	-	-	134.7	-	-	135.3	-	-
2	44.5	2.75	(2H, t, 8)	33.9	-	-	103.3	6.62	(1H, s)	103.2	6.61	(1H, s)
3	209.2	-	-	199.9	-	-	152.3	-	-	152.2	-	-
4	42.6	2.56	(2H, t, 8.0)	123.85.71	(1H, s)	-	128.7	-	-	128.5	-	-
5	27.2	2.47	(2H, q, 7.5)	172.0	-	-	152.3	-	-	152.2	-	-
6	128.9	6.16	(1H, dt, 7.0, 15.7)	33.1	-	-	103.3	6.62	(1H, s)	103.2	6.61	(1H, s)
7	130.9	6.38	(1H, d, 16)	32.1	-	-	134.1	6.58	(1H, d, 16.0)	130.9	6.54	(1H, d, 15.5)
8	141.1	-	-	35.8	-	-	123.7	6.23	(1H, dt, 16.0, 6.0)	129.1	6.30	(1H, dt, 15.5, 6.0)
9	128.4	7.17	(1H, m)	53.9	-	-	65.0	4.71	(2H, d, 6.0)	63.6	4.31	(2H, d, 6.0)
10	128.6	7.26	(1H, m)	38.7	-	-	56.2	3.82	(3H, s)	56.2	3.81	(3H, s)
11	127.2	7.26	(1H, m)	21.1	-	-	168.9	-	-	169.0	-	-
12	128.6	7.26	(1H, m)	39.7	-	-	20.6	2.23	(3H, s)	20.6	2.32	(3H, s)
13	128.4	7.17	(1H, m)	42.5	-	-	56.2	3.82	(3H, s)	56.2	3.81	(3H, s)
14	137.5	-	-	55.9	-	-	171.0	-	-	-	-	-
15	126.2	7.31	(1H, m)	28.3	-	-	21.1	2.10	(3H, s)	-	-	-
16	128.6	7.26	(1H, m)	24.3	-	-	-	-	-	-	-	-
17	126.1	7.17	(1H, m)	56.1	-	-	-	-	-	-	-	-
18	128.6	7.26	(1H, m)	12.10.69	(3H, s)	-	-	-	-	-	-	-
19	126.2	7.31	(1H, m)	17.51.17	(3H, s)	-	-	-	-	-	-	-
20	-	-	-	36.2	-	-	-	-	-	-	-	-
21	-	-	-	18.80.90	(3H, d, 6.7)	-	-	-	-	-	-	-
22	-	-	-	34.1	-	-	-	-	-	-	-	-
23	-	-	-	26.1	-	-	-	-	-	-	-	-
24	-	-	-	45.9	-	-	-	-	-	-	-	-
25	-	-	-	29.2	-	-	-	-	-	-	-	-
26	-	-	-	19.90.82	(3H, d, 7.3)	-	-	-	-	-	-	-
27	-	-	-	19.10.80	(3H, d, 6.7)	-	-	-	-	-	-	-
28	-	-	-	23.1	-	-	-	-	-	-	-	-
29	-	-	-	12.00.85	(3H, t, 7.2)	-	-	-	-	-	-	-

3.2. Cytotoxic Activity assay

Our cytotoxic activity assay using CCK-8 assay exhibited that the IC_{50} of 1,7-diphenyl-6-heptene-3-one, sitostenone, sinapyl alcohol diacetate, and sinapyl alcohol acetate against MDA-MB-231 cells were 134.59; 170; 128.11; and 161.96 $\mu\text{g}/\text{mL}$, respectively (**Figure 6**).

3.3. Migration Cell Assay

Followed with cytotoxicity assay, all isolates that provided anti-migration properties with sitostenone exhibited the lowest migration rate (%) compared to other isolates in every concentration (25, 50, 100, and 200 $\mu\text{g}/\text{mL}$). The migration rate is concentration-dependent and increases in concentration cause the decrement in migration (**Figures 7 and 8**). The lowest IC_{50} concentration was shown by sitostenon at 200 $\mu\text{g}/\text{mL}$ with a migration rate of 3.32%.

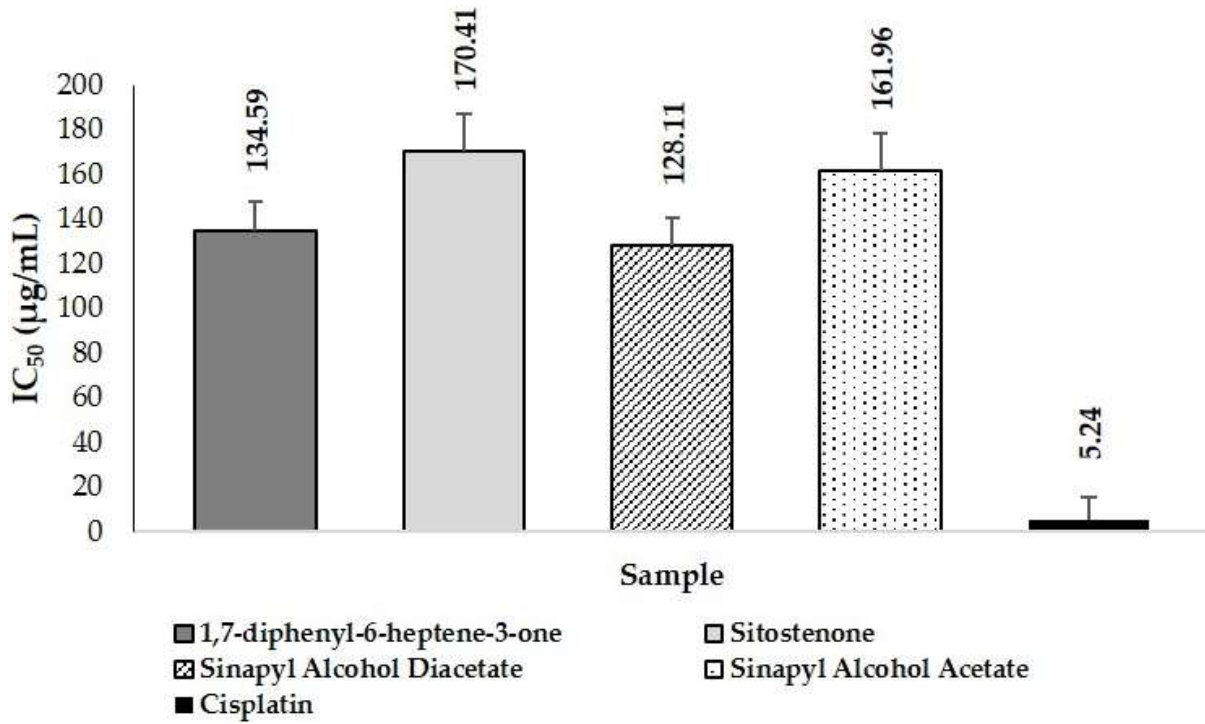


Figure 6. The IC₅₀ value of isolates.

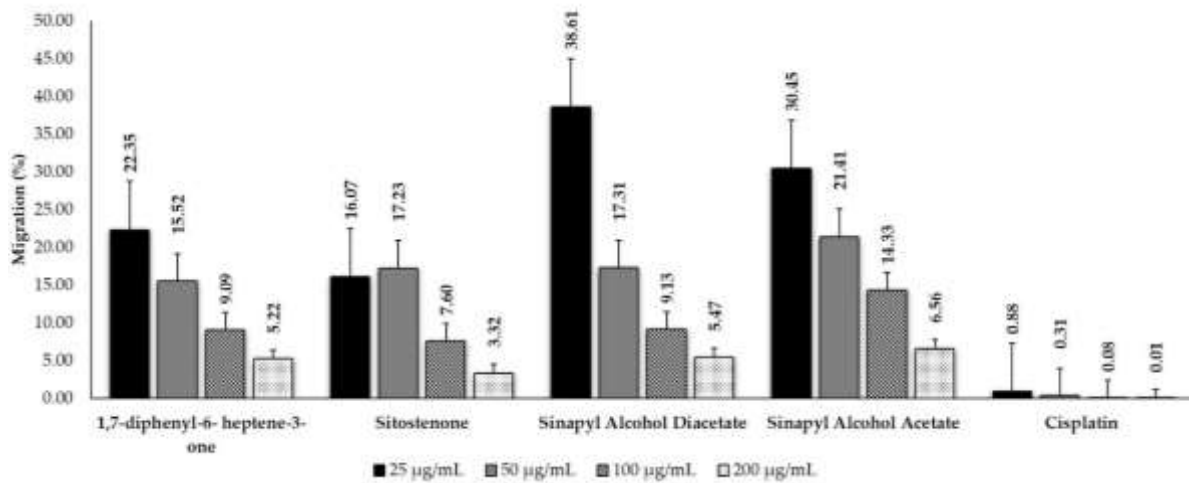


Figure 7. The migration rate of isolates.

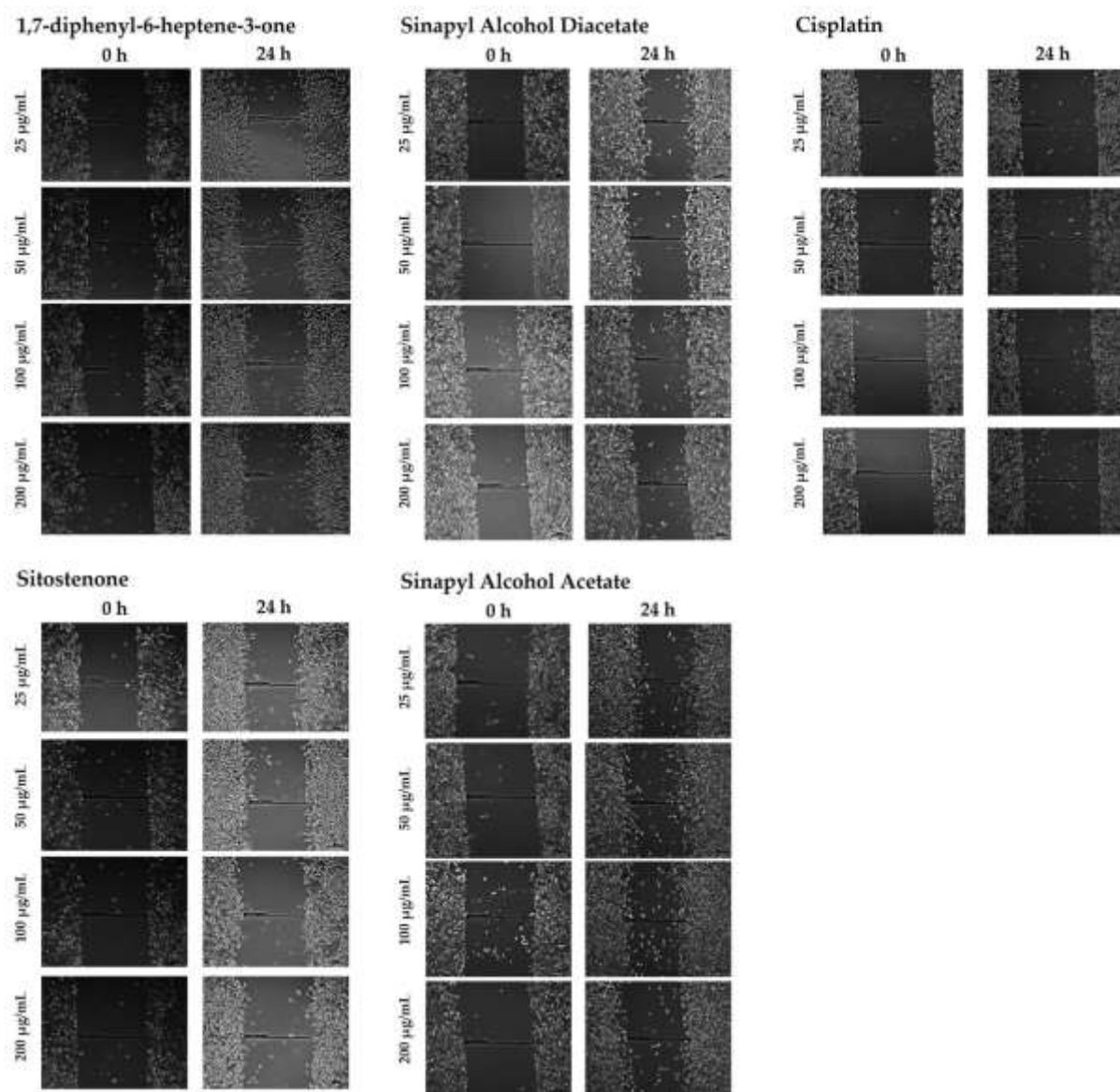


Figure 8. In vitro scratch assay (X 40 magnification) of MDA-MB231 cells towards isolates and Cisplatin in various concentrations (25 µg/mL; 50 µg/mL; 100 µg/mL; 200 µg/mL).

3.4. Molecular Docking

Here we performed molecular docking of RS2 (native ligand) to the MMP-1 enzyme to evaluate the ability of Autodock to mimic its x-ray pattern. The conformation of RS2 on redocking and x-ray results showed a similar position with an RMSD value of 1.155 Å (**Figure 9**). The RMSD criterion of the RS2 heavy atoms between the re-docked and experimental poses (crystallography) was used to determine the rationality of the docking procedure. An RMSD value below 2 Å establishes an excellent binding pose search quality (*Kasmawati et al., 2022*).

RS2 had binding energy of -9.99 kcal/mol, and four hydrogen bonds (H-bond) were observed with Leu181, Ala182, Glu219, and His228 residues. This interaction was formed from their carbonyl and hydroxyl groups. Meanwhile, residues of Leu181, Arg214, and Val215, as well as Zn atoms, showed hydrophobic and van der Waals interactions with RS2 (**Figure 10E**). The binding energy of all isolates can be seen in **Table 3**. Binding energy was used to evaluate a compound's affinity or ability to bind to target proteins. The stronger the compound's affinity, the more negative its binding energy value (*Arba et al., 2020*).

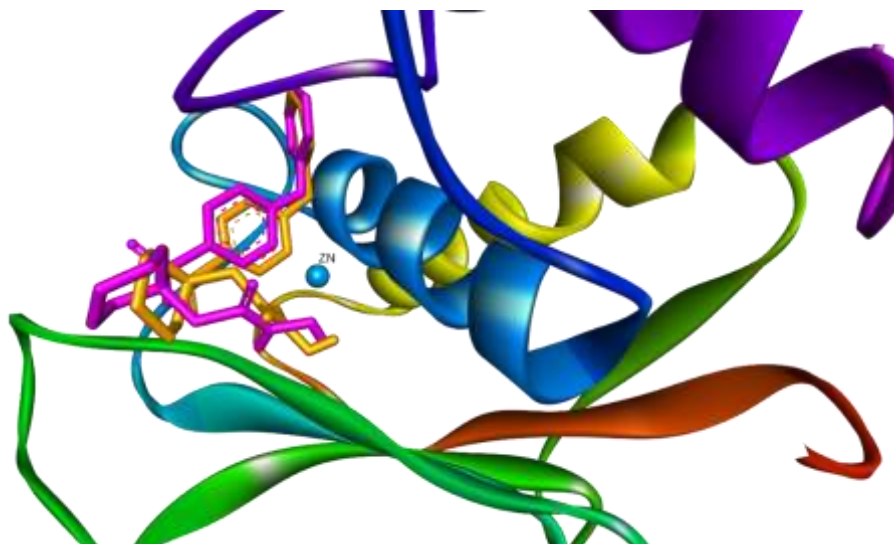


Figure 9. The docked poses of RS2 (pink) and x-ray (orange) in MMP-1.

Table 3. Summary binding energies of all isolates.

Compounds	Compounds Code	Binding energy (kcal/mol)
Sitostenon	lig_1	-11.81
1,7-diphenyl-6-heptene-3-one	lig_2	-8.25
Sinapyl Alcohol Acetate	lig_3	-6.64
Sinapyl Alcohol Diacetate	lig_4	-6.28
Cisplatin	-	-6.79
RS2 (Native ligand)	-	-9.99

Figure 10 depicts the best poses and interactions of the isolate compounds when bound to MMP-1's binding pocket. The observed interactions were dominated by van der Waals interactions, hydrogen bonds, and hydrophobic interactions. **Figure 10A** shows the best pose for lig 1 when it binds to the MMP-1. There was no H-bond in lig 1, but it had a non-bonding (van der Waals) interaction with the Zn atom on MMP-1's catalytic site. In addition, eight hydrophobic interactions with residues of Leu181, Arg214, Val215, His218, His228, Pro238, His222, and Tyr240 were also observed. Lig₂ had binding energy of -8.25 kcal/mol, slightly lower than lig₁ and RS2. In this compound, the carbonyl group played a vital role in forming two H-bond with Leu181 and Ala182 residues and the van der Waals interactions with Zn atoms on the MMP-1 binding site (**Figure 10B**). The benzene group of this compound formed

hydrophobic interactions with Arg214, His218, and His228 residues.

The lig₃ and lig₄ had similar binding energies of -6.64 kcal/mol and -6.28 kcal/mol, respectively. These two compounds formed H-bond at the carbonyl group and their hydrogen atoms, but mostly in lig 4 with the residues Leu181, Ala182, Glu219, His228, Tyr240, and Thr241 (**Figure 10C-10D**). In addition, the hydrophobic interactions were supported by benzene, hydroxy, and methyl groups in these two compounds with Leu181, His218, and Val215 residues. All isolated compounds were found to form van der Waals interactions with Zn atoms, which are required for MMP-1's catalytic process. Cisplatin used as a control in this study had more positive binding energy than lig₃ and lig₄. Cisplatin was known to form H-bond with residues Ala181 and hydrophobic interactions with His222 of MMP-1 (**Figure 10F**).

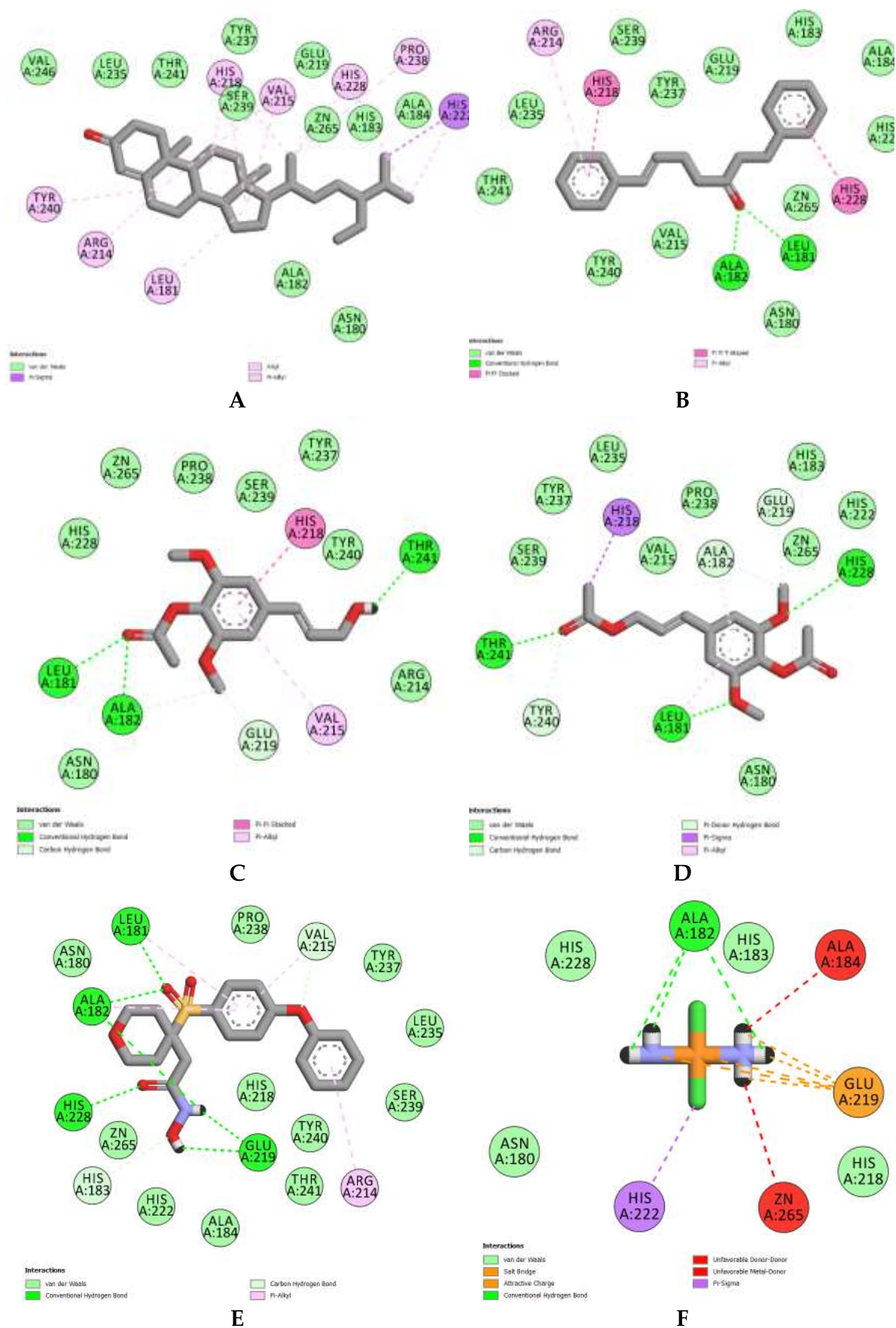


Figure 10. 2D interactions of (A) lig_1, (B) lig_2, (C) lig_3, (D) lig_4, (E) RS2, and (F) cisplatin with MMP-1.

3.5. Molecular Dynamics Simulation

3.5.1. RMSD analysis

The RMSD of the MMP-1 backbone and isolated compounds can be seen in **Figure 11**. RMSD compares the folded protein structure to the partially or wholly unfolded system in a protein simulation. The RMSD depicts the dynamic changes in the protein during the simulation, which are related to the protein's stability (Sargsyan et al., 2017). This figure shows that the RMSD backbone was more stable in the lig_2 complex than in the other complexes. The protein backbone of all complexes showed a similar trend with RMSD values of ~ 3 Å (**Figure 11B**).

In the MMP-1-lig_2 complex, a stable spine was observed during the simulation with an average RMSD of 2.96 Å. The MMP-1-lig_1 complex has an average RMSD of 2.93 Å. In this complex, during 0-32 ns, the protein increases to ~ 3.5 Å and the highest at ~ 25 ns by ~ 3.7 Å. At the end of the simulation, the trend decreased with a final RMSD value of ~ 2.9 Å (**Figure 11A**). The backbone movement in the MMP-1-lig_4 complex had an average RMSD of 2.83 Å. RMSD increased in this complex up to ~ 35 ns and stabilized until 50 ns (**Figure 11D**). In the complex MMP-1-lig_3, a similar trend was seen with the MMP-1-lig_4 with an average RMSD of 2.97 Å (**Figure 11C**). The protein spine in this complex began to stabilize at ~ 32 ns. In comparison, the backbone of MMP-1-RS2 and MMP-1-cisplatin was stable, with an average RMSD of 2.82 and 2.42 Å, respectively (**Figure 11E-F**).

In addition, we analyzed the RMSD pattern of each isolated compound during the simulation. The RMSD values of lig_1, lig_2, lig_3 and lig_4 was 1.52; 1.83; 0.65; and 1.07 Å, respectively. RMSD in lig_2 fluctuated at ~ 25 ns, then stabilized until the end of the simulation. lig_1, lig_4, and

lig_3 during the simulation showed excellent stability. There were fluctuations in lig_4 during the simulation time of ~ 30 ns but then stabilized until the end. Finally, the dynamics of RS2 and cisplatin were very different, where cisplatin is very stable from the beginning to the end of the simulation. At the same time, RS2 fluctuates, which tends to increase. The RS2 reached a point of stability at ~ 38 ns until the end. These results also illustrate that all isolate compounds were more able to stabilize MMP-1 than native ligands.

3.5.2. RMSF analysis

Analysis of the fluctuations (RMSF) of each residue in the MMP-1 backbone showed various movements (**Figure 12**). The RMSF characterizes the oscillation of the center C atoms in the protein structure by representing the fluctuation of the coordinates of each amino acid near its reference coordinate during the simulation process (Shao et al., 2022). Overall, RMSF was high in several residues such as Arg169, Pro177, Gly190, Arg202, Arg208, Arg214, Ile232, Phe242, Gln247, and Asp251. The N-terminus and C-terminus regions of MMP-1 (Arg108 and Gln264) displayed high peak intensity with fluctuation values of ~ 0.5 . Lig_2, lig_1, and lig_4 displayed similar RMSF trends without any fluctuations specific to any particular residue (**Figure 12A, 12B, and 12D**). In lig_3, changes in the MMP-1 backbone became more intense, such as in the Gly190 with an RMSF of 4.82 (**Figure 12C**). In addition, residues in the region 247-262 of this complex showed a reasonably high intensity. This situation illustrates that lig_3 affects the fluctuation of several residues in the MMP-1 backbone. However, overall complexes display similar fluctuation trends during the simulation.

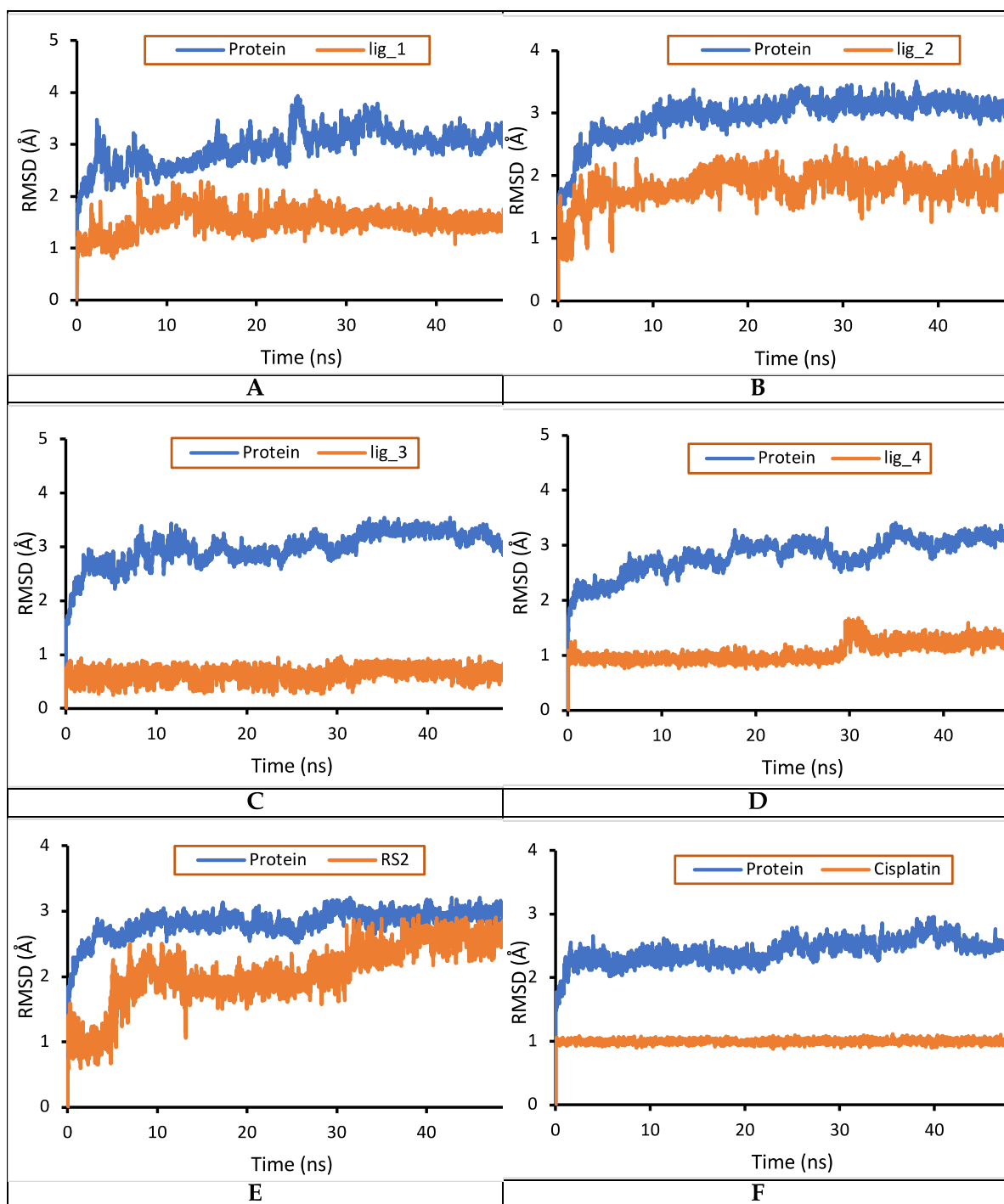


Figure 11. The RMSD graph of (A) complex lig_1, (B) complex lig_2, (C) complex lig_3, (D) complex lig_4, (E) complex RS2, and (F) complex cisplatin during 50 ns simulation.

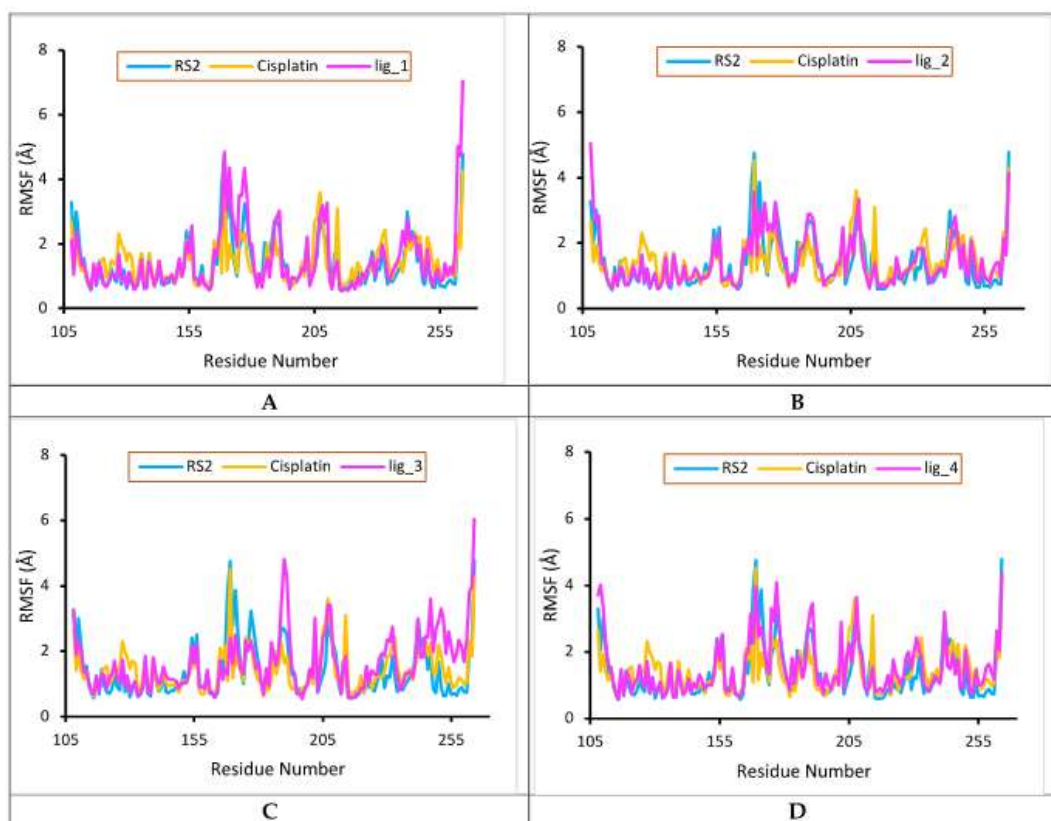


Figure 12. The RMSF plots of (A) lig_1, (B) lig_2, (C) lig_3, and (D) lig_4 compared to RS2 and cisplatin during 50 ns simulation.

3.5.2. SASA analysis

One of our concerns is the area that accessible by the solvents. These parameters can describe the complex's folding and stability during simulation-based changes in the protein solvent area (Savojardo et al., 2021) presented in **Figure 13**. The SASA area of RS2 and cisplatin was smaller than the isolated compound, with an average of 88.1 and 87.6 nm², respectively. Lig_2, lig_1, and lig_4 showed a constant area during the simulation with SASA averages of 89.7; 91.5; and 90.4 nm², respectively. **Figure 13** shows a decrease in the SASA area at ~20 ns in the lig_2 complex and ~30 ns in the lig_1 complex. However, the remaining simulation time for the SASA area remains constant. The difference was observed in the lig_3 complex, where the SASA area got smaller during the simulation to ~46 ns which then expanded to the end. The lig_3 complex had an average size of 88.7 nm². lig_3

causes a change in the area accessed by the solvent to the MMP-1.

3.5.3. Gyration radius analysis

Protein compactness during the simulation was determined by measuring the radius gyration of each complex (**Figure 14**). Low and constant protein radius of gyration (R_g) values characterized stable protein folding behavior during the simulation. The R_g value is defined as the distribution of its atoms around its axis. R_g is the length representing the distance between the rotating point and the point where energy transfer has the most significant effect. The calculation of R_g is the essential indicator widely used in predicting the structural activity of a macromolecule. When a ligand binds to the protein, the R_g changes due to a conformational change. A protein's compactness is directly related to its folding rate and impact on protein stability (Sneha, 2016). All complexes had

compactness with a range of R_g values of between 1.50 and 1.56 nm. The results showed that the lig_2 complex had an average R_g value of 1.527 nm. The study showed that the lig_2 and lig_1 complex had an average R_g value of 1.527 and 1.529 nm, but the lig_1 complex had a decrease

in the R_g value at a simulation time of ~30 ns to 1.50 nm. Lig_4 and lig_3 show a similar trend of R_g with average values of 1.524 and 1.536 nm, respectively. These results also showed that the lig_4 complex was the compound with the lowest R_g compared to other isolates.

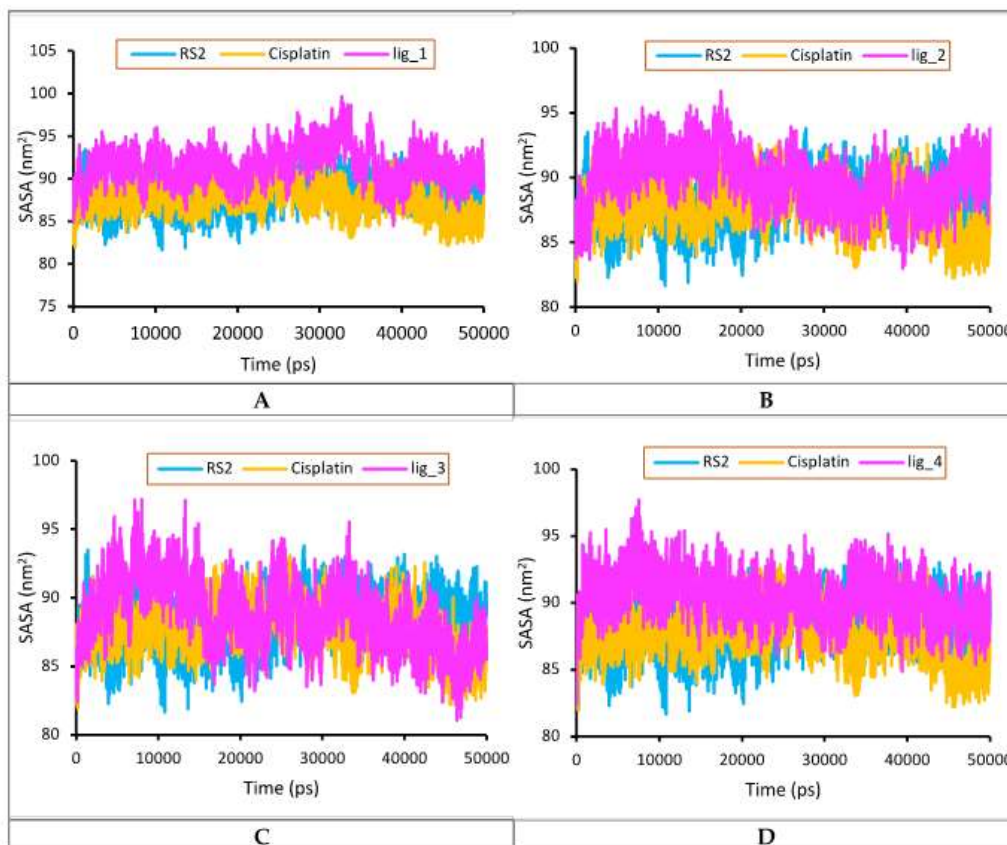


Figure 13. The SASA plots of (A) lig_1, (B) lig_2, (C) lig_3, and (D) lig_4 compared to RS2 and cisplatin during 50 ns simulation.

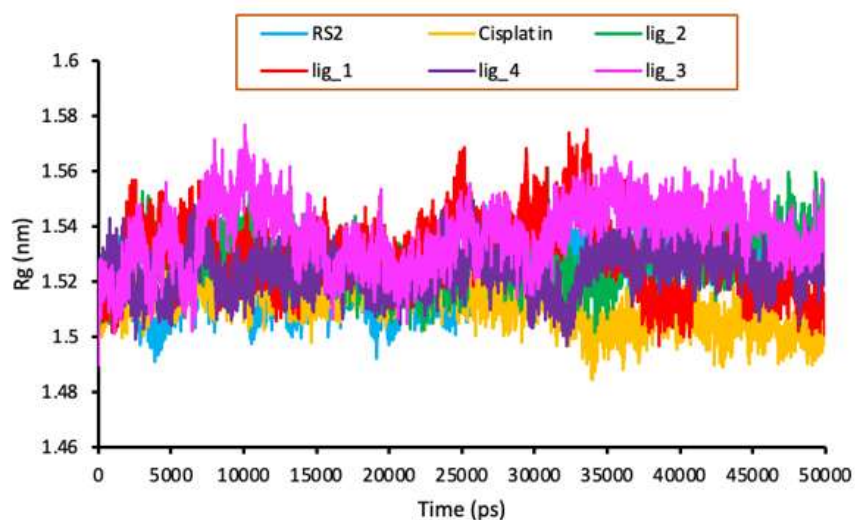


Figure 14. The gyration radius plot of all isolated compare to RS2 and cisplatin during 50 ns simulation.

3.5.4. Principal component analysis

We identified the overall essential movement trend of the complex based on principal component analysis (PCA). The protein backbone fluctuations were recorded in two eigenvectors and visualized on a 2D plot (**Figure 15**). PCA is a data extraction technique that uses a covariance matrix constructed from atomic coordinates that describe the accessible degrees of freedom (DOF) of the protein, such as Cartesian coordinates that define atomic displacements in each conformation comprising the path, to extract the essential elements in the

trajectory. An eigenvalue decomposition characterizes a portion of the motion, where larger eigenvalues describe protein movements on larger spatial scales (David & Jacobs, 2014). Stable complexes can be seen from the smaller space occupied by the cluster during the simulation. In the 2D eigenvector plot, the lig_2 complex was known to occupy a more expansive space, and lig_4 has the smallest cluster area of the other complexes. Interestingly, the lig_1 complex exhibited a cluster pattern similar to RS2 and cisplatin. In contrast, the lig_3 complex displayed a way with regions opposite RS2 and cisplatin but nearly the same cluster area.

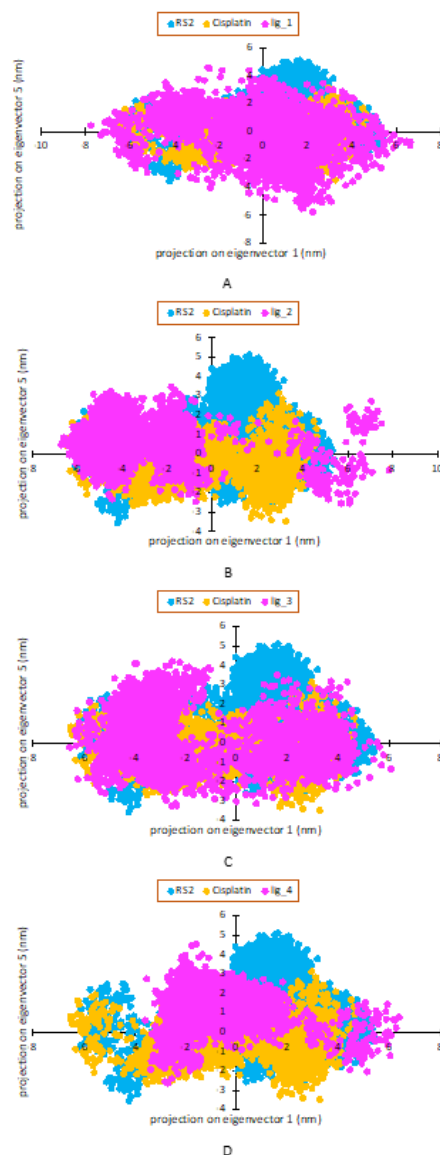


Figure 15. The 2D eigenvectors plots of (A) lig_1, (B) lig_2, (C) lig_3, and (D) lig_4 compared to RS2 and cisplatin during 50 ns simulation.

3.5.5. Protein-ligand interaction analysis

Hydrogen bond occupancy from protein-ligand interactions was also analyzed in the complex system of each compound. In the RS2 complex, H-bond interactions were observed at residues Leu181 (159.62%), Ala182 (73.08%), Val215 (86.54%), Hi118 (69.23%), and Tyr240 (101.92%). In our results, the cisplatin complex formed H-bond interactions with Leu181 and Ala182, which were less intense (< 10%). However, this compound has interesting H-bond interactions with residues Hi128 (88.46%), Hi122 (63.46%), and Glu219 (21.15%). In all isolates, Tyr240 residue formed a very intense H-bond interaction with more than 100% occupancy.

The lig_2 was observed to have a very intense occupancy H-bond with residues of Leu181 (119.23%), Thr241 (109.62%), and Val215 (111.54%). In addition, there was a fairly intense interaction with residues of Pro238 (75%) and Ala182 (44.23%). In the lig_1 complex, the most intense interaction was observed at residue Thr241 (118.46%). While the residues Arg214, Leu181, and Ala182 each had an interaction intensity of 80.77%, 59.62%, and 23.08%. H-bond occupancy of residues leu181, Ala182, Thr241, and Val215 from the lig_4 and lig_3 was also observed but with different intensities. In Leu181 and Ala182 residues, lig_3 formed a more intense bond (76.92% and 36.54%) than lig_4 (51.92% and 17.31%).

On the other hand, at residues Thr241 and Val215, lig_4 had a more intense H-bond by 50% and 82.69% than lig_3 by 48.08% and 67.31%, respectively. In addition, we also analyzed the interaction of each isolate against zinc ions on MMP-1. The results showed that RS2 formed an interaction with zinc ions by 19.23%. In contrast to cisplatin, this compound was observed with no interaction with ion Zn^{2+}

on the MMP-1 active site. The isolates lig_1 and lig_4 formed interactions with zinc ions by 32.69% and 11.54%, respectively. This result is quite high compared to the other two isolates, which were only 9.62% and 7.69% for lig_3 and lig_2, respectively.

3.5.6. MM-PBSA calculation

The binding energy of all isolates was calculated from molecular dynamics simulation based on the MM-PBSA method shown in **Table 4**. MM/PBSA was used to evaluate binding poses, determine structural stability, and predict binding affinity. Furthermore, MM/PBSA enables the analysis of individual energies that contribute to the detailed specific energy for system binding, identifies dominant interactions in the binding process, and supports drug design (Wang *et al.*, 2019).

The total binding energy (ΔE_{Bind}) for the RS2 and cisplatin systems was -83.73 kcal/mol and 563.59 kcal/mol, which was higher than the system of all isolates. The lowest binding energy was found by compound lig_1 followed by lig_4 at -176.83 kcal/mol and -99.74 kcal/mol, respectively. Slightly lower points but still better than RS2 were isolates lig_2 and lig_3 with binding energies of -91.09 kcal/mol and -86/47 kcal/mol. This study showed a better affinity for isolates for MMP-1 than RS2.

It was observed that the van der Waals (ΔE_{VDW}), electrostatic (ΔE_{Ele}), and SASA (ΔE_{SASA}) energies were essential factors to consider in contributing to the favorable binding of all systems. The electrostatic energy was more positive in the cisplatin and lig_2 systems but becomes more profitable in the lig_4 and RS2 systems. Meanwhile, the polar solvation energy (ΔE_{PB}) was less favorable in the system by making a more positive contribution to the binding energy.

Table 4. The binding energies of all systems during 50 ns simulation.

Compounds	ΔE_{VDW}	ΔE_{Ele}	ΔE_{PB}	ΔE_{SASA}	ΔE_{Bind}
Lig_1	-225.54 ± 27.74	-7.06 ± 5.28	76.57 ± 35.81	-20.80 ± 2.01	-176.83 ± 30.50
Lig_2	-159.42 ± 11.54	-17.20 ± 12.03	101.05 ± 30.39	-15.51 ± 1.09	-91.09 ± 26.49
Lig_3	-148.09 ± 10.48	-14.16 ± 11.32	89.91 ± 16.52	-14.13 ± 0.81	-86.47 ± 12.40
Lig_4	-162.93 ± 12.34	-41.74 ± 10.95	122.04 ± 24.59	-17.10 ± 0.95	-99.74 ± 25.52
RS2	-156.62 ± 14.86	-23.69 ± 20.20	111.18 ± 28.89	-14.60 ± 1.22	-83.73 ± 24.80
Cisplatin	-23.14 ± 12.26	632.28 ± 29.92	-41.55 ± 32.60	-6.99 ± 0.50	562.59 ± 31.14

4. DISCUSSION

Four compounds (1-4) were isolated and identified from the ethanol extract of *E. alba* rhizome, which are

- (i) 1,7-diphenyl-6-heptene-3-one;
- (ii) Sitostenon;
- (iii) Sinapyl Alcohol Diacetate;
- (iv) Sinapyl Alcohol Acetate.

Our results suggest that isolated compounds from *Etingera alba* have anticancer activity. The ability of the sinapyl alcohol diacetate (3) which is better in providing activity than other compounds is due to the influence of the carbonyl group. Sinapyl alcohol diacetate (3) has two carbonyl groups while other compounds have only one carbonyl group.

The carbonyl group can provide activity as an antioxidant. It has the potential to increase its anticancer activity. Compounds with a carbonyl group have a stronger ability to induce apoptosis than compounds without a carbonyl group (Rahman et al., 2018).

According to the previous study, the 1,7-diphenyl-6-heptene-3-one that belonged to the diarylheptanoid compound showed cytotoxic activity against MCF-7 cell lines (Winuthayanon et al., 2009). Diarylheptanoid compounds act as antiproliferative of cell cancer by

inhibiting topoisomerase I and II in cancer cells (Rahman et al., 2018).

In other studies, diarylheptanoid compounds potently provided cytotoxic activity against the IMR-32 human neuroblastoma cell line by inhibiting PAF receptor binding and inducible NO synthase protein and suppressing the mRNA expression (Sun et al., 2008). Sitostenone is a phytosterol compound with anticancer activity against Hela, A549, and HepG2 by inhibiting the cell cycle at the G0/G1 phase (Zhou et al., 2018).

Previous studies also showed that sterols possess cytotoxicity activity against colorectal cancer (HCT-116), hepatocellular carcinoma (HepG-2), and prostate cancer (PC-3) cell lines (Abdel-Mageed et al., 2021). Both sinapyl alcohol acetate and sinapyl alcohol diacetate belong to the phenylpropanoid compound. Both are analog to cinnamic acid, which is reported to have anticancer activity and invasion, migration, and adhesion (Hunke et al., 2018).

The previous study showed that sitostenone from *Etingera elatior* exhibited high antitumor-promoting activity (Habsah et al., 2005). The migration cell rate mimics invasion of the basement membrane and cell migration in metastasis progression (Hapach et al., 2019).

Our result suggests that sitostenon also provides anti-metastatic inhibition in the migration of cell cancer. The migration inhibition process is shown in **Figure 8**. The mechanism is unclear; however, it might have a similar mechanism to Cisplatin in inhibiting the migration process.

Cisplatin was used as a control in migration assay due to its ability to inhibit filopodia formation induced by transforming growth factor-beta (TGF- β). TGF- β is a growth factor that acts as a metastasis promoter in cell cancer (Wang *et al.*, 2021). The other mechanism proposed by the sitostenon is by inhibiting the MMP-9 (matrix metalloproteases-9) expression and activity, as MMP-9 is playing a vital role in metastasis by disrupting the extracellular matrix. MMP-9 is highly expressed in invasive breast cancer (Maxwell *et al.*, 2017).

We also investigated MMP-1 inhibition to provide a molecular profile of the anti-migration mechanism of the four isolates based on molecular docking and dynamics simulation. MMP-1 is known to increase the release of growth factors that impact the occurrence of cancer cell metastasis, so inhibition of the function of MMP-1 is expected to reduce breast cancer cell invasion (Liu *et al.*, 2012). Based on the docking study, it was found that four isolated compounds could bind to the catalytic site of MMP-1 with the best affinity for lig_1 compared to RS2. This study showed that the isolates interacted with catalytic residues such as Leu181, Ala182, Arg214, Glu219, and Tyr240 in MMP-1 (Lovejoy *et al.*, 1999). This residue is responsible for the formation of bonded and non-bonded interactions.

Dynamic studies of the MMP-1-isolate complexes provided information regarding their stability, flexibility, and binding affinity. We observed that the binding pattern of each complex was very stable, based on RMSD, RMSF, SASA, *Rg*, and PCA analysis.

The highest intensity residual movement of the MMP-1 backbone was seen in Gly190 of lig_3. Meanwhile, the spine's N-terminus (Arg158) and C-terminus (Gln264) regions also showed high fluctuations. The isolated compound showed similar protein conformational changes when RS2 binds to MMP-1, especially in lig_1. In PCA analysis, lig_1 displays clusters similar to RS2 and cisplatin. Prediction of the binding energy of the isolated compound was predicted to be better than RS2 and cisplatin, especially lig_1. Lig_1 showed results that were in line with in vitro tests on the migration of cancer cells. This compound was found to have the best activity in inhibiting cancer cell migration than the other isolate. One of these results is supported by the interaction with Zn²⁺ ions at the MMP-1 catalytic site, where lig_1 has the highest intensity compared to other compounds, with a presentation of 32.69%.

This ion is one of the catalytic domains that play an essential role in the activity of MMP-1, so binding to this ion can inhibit the activity of MMP-1 and act as an anti-migration from cancer cells (Laronha & Caldeira, 2020). Our findings are preliminary data in metastasis breast cancer stage, which is migration and invasion. To complete the data, molecular in vitro, and in vivo experiment is suggested, especially in the MMP-1 pathway, which plays a vital role in the metastasis of breast cancer.

5. CONCLUSION

Compounds from *E. alba* rhizomes, including 1,7-diphenyl-6-heptene-3-one, Sitostenon, Sinapyl Alcohol Diacetate, and Sinapyl Alcohol Acetate have promising compounds to be developed as anticancer and anti-metastatic for TNBC. The most potential compounds shown by Sinaphyl alcohol diacetate exhibited the highest cytotoxic activity, and sitostenon exhibited the lowest cell migration related to its

antimetastatic activity. In addition, the docking and molecular dynamics showed that steroid has a promising compound for inhibiting MMP-1, which is associated with TNBC metastatic activity based on docking results, dynamic stability, and binding energy by MMPBSA analysis.

6. ACKNOWLEDGMENTS

We acknowledge the support received from the Faculty of Pharmacy, Universitas

Halu Oleo, and the Faculty of Pharmacy, Universitas Padjadjaran.

7. AUTHORS' NOTE

The author(s) declare(s) that there is no conflict of interest regarding the publication of this article. The authors confirmed that the data and the paper are free of plagiarism

8. REFERENCES

- Abdel-Mageed, W. M., El-Gamal, A. A., Al-Massarani, S. M., Basudan, O. A., Badria, F. A., Abdel-Kader, M. S., Al-Rehaily, A. J., and Aati, H. Y. (2021). Sterols and triterpenes from *dobera glabra* growing in Saudi Arabia and their cytotoxic activity. *Plants (Basel, Switzerland)*, 10(1), 1-12.
- Abraham, M. J., Murtola, T., Schulz, R., Páll, S., Smith, J. C., Hess, B., Lindahl, E. (2015). GROMACS: High performance molecular simulations through multi-level parallelism from laptops to supercomputers. *SoftwareX*, 1(2), 19-25.
- Arba, M., Arfan, A., Trisnawati, A., and Kurniawati, D. (2020). Pharmacophore modeling to identify heat shock proteins-9 (HSP-90) inhibitors. *Galenika Journal of Pharmacy*, 6(2), 229-236.
- Argote Camacho, A. X., González Ramírez, A. R., Pérez Alonso, A. J., Rejón García, J. D., Olivares Urbano, M. A., Torné Poyatos, P., Ríos Arrabal, S., and Núñez, M. I. (2021). Metalloproteinases 1 and 3 as potential biomarkers in breast cancer development. *International Journal of Molecular Sciences*, 22(16), 1-15.
- Chan, E. W. C., Lim, Y. Y., and Wong, S. K. (2011). Phytochemistry and pharmacological properties of *Etlingera elatior*: A review. *Pharmacognosy Journal*, 3, 6-10.
- Chmielewska-Kassassir, M., Sobierajska, K., Ciszewski, W. M., Bukowiecka-Matusiak, M., Szczesna, D., Burzynska-Pedziwiatr, I., Wiczowski, W., Wagner, W., and Wozniak, L. A. (2020). Polyphenol extract from evening primrose (*Oenothera paradoxa*) inhibits invasion properties of human malignant pleural mesothelioma cells. *Biomolecules*, 10(11), 1-17.
- da Silva, J. L., Cardoso Nunes, N. C., Izetti, P., de Mesquita, G. G., and de Melo, A. C. (2020). Triple negative breast cancer: A thorough review of biomarkers. *Critical Reviews in Oncology/Hematology*, 145, 102855.
- David, C.C., and Jacobs, D.J. (2014). Principal component analysis: A method for determining the essential dynamics of proteins protein dynamics. *Methods in Molecular Biology*, 1084, 193-226.
- Fristiohady, A., Sadrun, B., Wahyuni, Yusuf, M.I., Malik, F., Purnama L.O.M.J., Bafadal, M., Leorita, M., Jabbar, A., and Sahidin, I. (2020), Hepatoprotective activity etlingera elatior

- (Jack) R.M. Smith extract against CCl₄-induced hepatic toxicity in male wistar rats, *Research journal of Pharmacy and Technology*, 13(10), 4585-4590.
- Habsah, M., Ali, A., Lajis, N., Sukari, M., Yap, Y., Kikuzaki, H., and Nakatani, N. (2005). Antitumour-promoting and cytotoxic constituents of *etlingera elatior*. *The Malaysian Journal of Medical Sciences: MJMS*, 12(1), 6–12.
- Hamsidi, R. Wahyuni, W., Sahidin, I., Apriyani, A., Harsono, H., Azizah, N. A., Malik, F., Yodha, A. W. M., Purnama, L. O. M. J., and Fristiohady, A. (2021). Suppression of proinflammatory cytokines by *etlingera alba* (A.D.) Poulsen rhizome extract and its antibacterial properties. *Advances in Pharmacological and Pharmaceutical Sciences*, 2021, 1-6.
- Hapach, L. A., Mosier, J. A., Wang, W., and Reinhart-King, C. A. (2019). Engineered models to parse apart the metastatic cascade. *NPJ Precision Oncology*, 3(1), 1-8.
- Hunke, M., Martinez, W., Kashyap, A., Bokoskie, T., Pattabiraman, M., and Chandra, S. (2018). Antineoplastic actions of cinnamic acids and their dimers in breast cancer cells: A comparative study. *Anticancer Research*, 38(8), 4469–4474.
- Jabbar A, Wahyuono S, Sahidin I, and Puspitasari, I. (2021). Free radical scavenging activity of methanol extracts and compounds isolated from the stems of *etlingera rubroloba* AD poulsen. *International Journal of Pharmaceutical*, 13(1), 1099-1105.
- Kasmawati, H., Mustarichie, R., Halimah, E., Ruslin, R., Arfan, A., and Sida, N.A. (2022). Unrevealing the potential of *sansevieria trifasciata* prain fraction for the treatment of androgenetic alopecia by inhibiting androgen receptors based on LC-MS/MS analysis, and in-silico studies. *Molecules*, 27(14), 1-12.
- Kumari, R., and Kumar, R. (2014). Open source drug discovery consortium, and Lynn, A. g_mmpbsa--a GROMACS tool for high-throughput MM-PBSA calculations. *Journal of Chemical Information and Modeling*, 54(7), 1951–1962.
- Laronha, H., and Caldeira, J. (2020). Structure and function of human matrix metalloproteinases. *Cells*, 9(5), 1-18.
- Liu, H., Kato, Y., Erzinger, S. A., Kiriakova, G. M., Qian, Y., Palmieri, D., Steeg, P. S., and Price, J. E. (2012). The role of MMP-1 in breast cancer growth and metastasis to the brain in a xenograft model. *BMC Cancer*, 12, 1-11.
- Liu, L., Yan, J., Cao, Y., Yan, Y., Shen, X., Yu, B., Tao, L., and Wang, S. (2021). Proliferation, migration and invasion of triple negative breast cancer cells are suppressed by berbamine via the PI3K/Akt/MDM2/p53 and PI3K/Akt/mTOR signaling pathways. *Oncology Letters*, 21(1), 1-10.
- Lovejoy, B., Welch, A. R., Carr, S., Luong, C., Broka, C., Hendricks, R. T., Campbell, J. A., Walker, K. A., Martin, R., Van Wart, H., and Browner, M. F. (1999). Crystal structures of MMP-1 and -13 reveal the structural basis for selectivity of collagenase inhibitors. *Nature Structural Biology*, 6(3), 217–221.
- Mahdavi, B. (2014). Chemical constituents of the aerial parts of *Etlingera brevilabrum* (zingiberaceae). *Der Pharma Chemica*, 6, 360-365.

- Maxwell, T., Chun, S. Y., Lee, K. S., Kim, S., and Nam, K. S. (2017). The anti-metastatic effects of the phytoestrogen arctigenin on human breast cancer cell lines regardless of the status of ER expression. *International Journal of Oncology*, 50(2), 727–735.
- Morris, G. M., Huey, R., and Olson, A. J. (2008). Using autodock for ligand-receptor docking. *Current Protocols in Bioinformatics*, 24(1), 8-14.
- Morris, G. M., Huey, R., Lindstrom, W., Sanner, M. F., Belew, R. K., Goodsell, D. S., and Olson, A. J. (2009). AutoDock4 and AutoDockTools4: Automated docking with selective receptor flexibility. *Journal of Computational Chemistry*, 30(16), 2785–2791.
- Nagappan, T., Tatin, Y., and Skornickova, J. L. (2019). Investigation on bioactive potential of selected wild ginger, genus *etlingera* from Tasik Kenyir, Terengganu. *Greater Kenyir Landscapes*, 2019,75-82.
- Nandiyanto, A. B. D., Oktiani, R., and Ragadhita, R. (2019). How to read and interpret FTIR spectroscopy of organic material. *Indonesian Journal of Science and Technology*, 4(1), 97-118.
- Obinna, E. M. (2022). Physicochemical properties of human hair using Fourier transform infrared (FTIR) and scanning electron microscope (SEM). *ASEAN Journal for Science and Engineering in Materials*, 1(2), 71-74.
- Petrov, D., and Zagrovic, B. (2014). Are current atomistic force fields accurate enough to study proteins in crowded environments?. *PLoS Computational Biology*, 10(5), e1003638.
- Rahman, A. M., Lu, Y., Lee, H. J., Jo, H., Yin, W., Alam, M. S., Cha, H., Kadi, A. A., Kwon, Y., and Jahng, Y. (2018). Linear diarylheptanoids as potential anticancer therapeutics: Synthesis, biological evaluation, and structure-activity relationship studies. *Archives of Pharmacal Research*, 41(12), 1131–1148.
- Sahidin I., Wahyuni, Malaka M.H., Jabbar A., Imran and Manggau, M.A (2018). Evaluation of antiradical scavenger activity of extract and compounds from *etlingera calophrys* stems. *Asian Journal Of Pharmaceutical and Clinical Research*, 11(2), 238-241.
- Sahidin, I., Wahyuni, Rahim, A.R., Arba, M., Yodha, A.W.M., Rahmatika, N.S., Sabandar, C.W., Manggau, A.M., Khalid, R.M., Almuqarobbun, L.O.M.R., Rosandy, A.R., Chahyadi, A., Hartati, R., and Elfahmi. (2022). Radical scavenger and antimicrobe of diarylheptanoids and steroids from *etlingera calophrys* rhizome. *Sustainable Chemistry and Pharmacy*, 29, 100767.
- Sargsyan, K., Grauffel, C., and Lim, C. (2017). How molecular size impacts RMSD applications in molecular dynamics simulations. *Journal of Chemical Theory and Computation*, 13(4), 1518–1524.
- Sarkar, S., Horn, G., Moulton, K., Oza, A., Byler, S., Kokolus, S., and Longacre, M. (2013). Cancer development, progression, and therapy: an epigenetic overview. *International Journal of Molecular Sciences*, 14(10), 21087–21113.
- Savojardo, C., Manfredi, M., Martelli, P. L., and Casadio, R. (2021). Solvent accessibility of residues undergoing pathogenic variations in humans: From protein structures to protein sequences. *Frontiers in Molecular Biosciences*, 7, 626363.

- Shao, D., Zhang, Q., Xu, P., and Jiang, Z. (2022). Effects of the temperature and salt concentration on the structural characteristics of the protein (PDB Code 1BBL). *Polymers*, 14(11), 1-10.
- Sneha, P. (2016). Molecular dynamics: New frontier in personalized medicine personalized medicine. *Advances in Protein Chemistry and Structural Biology*, 102, 181-224.
- Sousa da Silva, A. W., and Vranken, W. F. (2012). ACPYPE - antechamber python parser interface. *BMC Research Notes*, 5(1), 1-8.
- Sukamto, S., and Rahmat, A. (2023). Evaluation of FTIR, macro and micronutrients of compost from black soldier fly residual: in context of its use as fertilizer. *ASEAN Journal of Science and Engineering*, 3(1), 21-30.
- Sun, Y., Tabata, K., Matsubara, H., Kitanaka, S., Suzuki, T., and Yasukawa, K. (2008). New cytotoxic diarylheptanoids from the rhizomes of *Alpinia officinarum*. *Planta Medica*, 74(4), 427-431.
- Sung, H., Ferlay, J., Siegel, R. L., Laversanne, M., Soerjomataram, I., Jemal, A., and Bray, F. (2021). Global cancer statistics 2020: Globocan estimates of incidence and mortality worldwide for 36 cancers in 185 countries. *CA: a Cancer Journal for Clinicians*, 71(3), 209-249.
- Tachai, S., and Nuntawong, N. (2016). Uncommon secondary metabolites from *Etingera pavieana* rhizomes. *Natural Product Research*, 30(19), 2215-2219.
- Wahyuni, Diantini, A., Ghozali, M., Subarnas, A., Julaeha, E., Amalia, R., and Sahidin, I. (2021a). Phytochemical screening, toxicity activity and antioxidant capacity of ethanolic extract of *etlingera alba* rhizome. *Pakistan Journal of Biological Sciences : PJBS*, 24(7), 807-814.
- Wahyuni, Grashella, S.H.L., Fitriah, W.O.I., Malaka M.H., Fristiohady A., Imran, and Sahidin, I. (2019). Antibacterial and antioxidant potentials of methanol extract and secondary metabolites from *Wualae* rhizome (*Etingera elatior*). *Current Research Bioscience and Biotechnology*, 1(1), 13-16.
- Wahyuni, W., Diantini, A., Ghozali, M., Subarnas, A., Julaeha, E., Amalia, R., and Sahidin, I. (2021b). Cytotoxic and antimigration activity of *etlingera alba* (a.d.) poulsen rhizome. *Advances in Pharmacological and Pharmaceutical Sciences*, 2021, 6597402.
- Wang, E., Sun, H., Wang, J., Wang, Z., Liu, H., Zhang, J., and Hou, T. (2019). End-point binding free energy calculation with MM/PBSA and MM/GBSA: Strategies and applications in drug design. *Chemical Reviews*, 119(16), 9478-9508.
- Wang, H., Gao, X., and Fang, J. (2016). Multiple staggered mesh ewald: Boosting the accuracy of the smooth particle mesh ewald method. *Journal of Chemical Theory and Computation*, 12(11), 5596-5608.
- Wang, H., Guo, S., Kim, S. J., Shao, F., Ho, J., Wong, K. U., Miao, Z., Hao, D., Zhao, M., Xu, J., Zeng, J., Wong, K. H., Di, L., Wong, A. H., Xu, X., and Deng, C. X. (2021). Cisplatin prevents breast cancer metastasis through blocking early EMT and retards cancer growth together with paclitaxel. *Theranostics*, 11(5), 2442-2459. <https://doi.org/10.7150/thno.46460>

- Wang, Q. M., Lv, L., Tang, Y., Zhang, L., and Wang, L. F. (2019). MMP-1 is overexpressed in triple-negative breast cancer tissues and the knockdown of MMP-1 expression inhibits tumor cell malignant behaviors in vitro. *Oncology Letters*, 17(2), 1732–1740.
- Winuthayanon, W., Piyachaturawat, P., Suksamrarn, A., Ponglikitmongkol, M., Arao, Y., Hewitt, S. C., and Korach, K. S. (2009). Diarylheptanoid phytoestrogens isolated from the medicinal plant *Curcuma comosa*: Biologic actions in vitro and in vivo indicate estrogen receptor-dependent mechanisms. *Environmental Health Perspectives*, 117(7), 1155–1161.
- Zhou, J., Li, G., Deng, Q., Zheng, D., Yang, X., and Xu, J. (2018). Cytotoxic constituents from the mangrove endophytic *pestalotiopsis* sp. induce G₀/G₁ cell cycle arrest and apoptosis in human cancer cells. *Natural Product Research*, 32(24), 2968–2972.